A method to enhance thickness and current-carrying capacity of BZO-doped YBCO multilayers

M. M. Aye, E. Rivasto, H. Rijckaert, H. Huhtinen and P. Paturi

***Abstract*—This study demonstrates a significant enhancement in the in-field critical current density and its isotropy in BZO-doped YBCO multilayer structures, achieved through improvements in the crystalline quality of YBCO, which extend the electron mean free path. The incorporation of undoped YBCO, alongside alternating BZO-doped and Ca-doped YBCO layers, revealed that the Ca-doped intermediate layer positively influenced the interface quality, promoting better growth in the subsequent layers. These improvements also enabled an increase in total film thickness, thereby enhancing the current-carrying capacity. Furthermore, the paper discusses the mechanisms behind these enhancements and presents a model explaining how nanorod pinning centres in different layers affect vortex pinning behavior. These insights offer valuable guidance for designing future YBCO coated conductor structures.**

***Index Terms*—HTS, YBCO, multilayers, thin film growth, crystalline quality, flux pinning, critical current density**

THE development of high-temperature superconducting (HTS) films, specifically $YBa_2Cu_3O_{6+x}$ (YBCO) films, for use in advanced electrical power applications, demands materials capable of operating efficiently under varied and demanding conditions [1]–[7]. This requirement highlights the need for YBCO films with high critical current densities (J_c) that are resistant against magnetic fields at varying temperatures. Achieving elevated in-field $J_c(B)$ in YBCO involves optimizing several material properties, chiefly among them are the crystalline quality and the effectiveness of flux pinning mechanisms [8]–[14].

Recent research underscores that while increasing the thickness of YBCO films can enhance the absolute critical current, it concurrently degrades crystalline quality and flux pinning properties beyond a certain critical thickness [15], [16]. At these greater thicknesses, the gradual relief of substrate-induced strain leads to a significant increase in crystal defects, which adversely affect the material's superconducting properties. To circumvent these limitations, the focus has shifted toward the design and fabrication of multilayer YBCO structures, where strategic layering is utilized to preserve crystalline integrity and enhance flux pinning without the adverse effects of increased thickness [14], [17]–[21]. Advancements in this field have shown that introducing an intermediate layer of Ca-doped YBCO (Ca-YBCO) can significantly reduce microstrain and other crystalline defects while preserving optimal oxygen content in the lattice. Specifically, the Ca-YBCO layer provides an ideal substrate for BZO-doped YBCO by reducing lattice mismatch by 30% when compared with undoped YBCO, thereby effectively minimizing interlayer strain. This improvement enhances both structural stability and overall crystalline quality [21]–[24]. This configuration not only improves the self-field $J_c(0)$ but also supports the growth of $BaZrO_3$ (BZO) nanorods. These nanorods serve as effective flux pinning centers, ideally extending through the entire film thickness in a well-ordered fashion [15], [25]–[30]. However, maintaining the alignment and continuity of BZO nanorods becomes challenging as film thickness increases, leading to diminished pinning effectiveness when these structures fracture or misalign [19], [28], [31], [32].

In this study, we aim to leverage previous findings by constructing multilayer YBCO structures, integrating BZO-doped YBCO layers with intermediate Ca-YBCO layers. This approach is designed to examine the feasibility of stacking multiple layers without degrading the films' structural and superconducting properties. Furthermore, we explore how BZO nanorods, distributed across different layers, influence overall flux pinning and how their arrangement might affect the anisotropy of the critical current density. This investigation into the structural and superconducting performance of YBCO multilayers doped with BZO aims to pave the way for the next generation of HTS materials tailored for enhanced performance in electric power applications.

I. Experimental details

The multilayers comprised an APC-free YBCO layer (0BZO, ≈40 nm), with an increasing number of alternating layers: 4% BZO-doped YBCO layers (4BZO, ≈65 nm) and 30% Ca-doped YBCO layers (Ca-YBCO, ≈15 nm). These layers were deposited using pulsed laser deposition (PLD) onto single crystal $SrTiO_3$ (STO) substrates, as depicted in Fig. 1(a) [7], [21]. Film thicknesses were measured by atomic force microscopy on strips etched for resistivity measurements, with individual layer thicknesses calibrated from transmission electron microscopy images. The naming convention for the multilayers was based on the number of 4BZO layers, denoted as 2x4BZO, 3x4BZO, 4x4BZO, and 5x4BZO, with total thicknesses of approximately 185 nm, 265 nm, 345 nm, and

Manuscript received November 5, 2024. This work was supported by the Jenny and Antti Wihuri Foundation. The authors thank Dr. N. Claes and Prof. S. Bals (University of Antwerp) for TEM measurements. H. R. acknowledges support and funding as a postdoctoral fellow of fundamental research from the Research Foundation—Flanders (FWO) under Grant No. 1273621N.

M. M. Aye, H. Huhtinen and P. Paturi are with the Wihuri Physical Laboratory, Department of Physics and Astronomy, University of Turku, FI-20014 Turku, Finland, (Email: hannu.huhtinen@utu.fi).

E. Rivasto is with the Wihuri Physical Laboratory, Department of Physics and Astronomy, University of Turku, FI-20014 Turku, Finland, also with the CP3-Origins, University of Southern Denmark, Campusvej 55, 5230 Odense M, Denmark.

H. Rijckaert is with the SCRiPTS, Department of Chemistry, Ghent University, 9000 Ghent, Belgium.

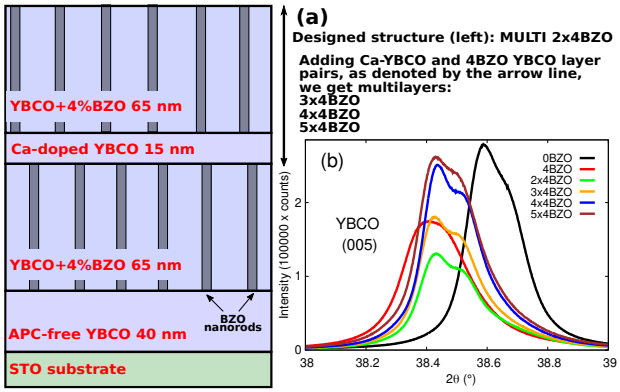

Fig. 1. (a) The schematic depicts multilayer structures, initiated with a ≈40 nm thick APC-free YBCO layer (0BZO) deposition on STO substrates, followed by an increasing number of alternating ≈65 nm thick BZO-doped YBCO layers (4BZO) and ≈15 nm Ca-doped YBCO layers. These multilayer samples are denoted by the number of BZO-doped YBCO layers, namely 2x4BZO, 3x4BZO, 4x4BZO, and 5x4BZO, thereby augmenting the total thickness of the multilayer structure. Additionally, individual layers of 0BZO and 4BZO were grown for comparative purposes, with their thickness matching that of the 5x4BZO multilayer structure. (b) Evolution of the Cu $K_{\alpha1/\alpha2}$ XRD 2θ (005) peak pairs in YBCO multilayer structures, along with single-layer 0BZO and 4BZO films for comparison.

TABLE I

STRUCTURAL PROPERTIES OF THE YBCO MULTILAYER STRUCTURES AND SINGLE-LAYER FILMS AS DETERMINED BY XRD MEASUREMENTS. THE FIRST FIVE COLUMNS PERTAIN TO THE YBCO (005) OR (102) PEAKS, WHILE THE LAST COLUMN DENOTES THE BZO (002) PEAK. THE TERM I_{ratio} REPRESENTS THE INTENSITY RATIO OF PEAKS $I(005)/I(004)$, INCREASE OF WHICH IS CLOSELY ASSOCIATED WITH OXYGEN DEFICIENCY WITHIN THE YBCO LATTICE [36].

Sample	c(Å)	$\Delta\theta(^\circ)$	$\Delta\phi(^\circ)$	$\Delta\omega(^\circ)$	I_{ratio}	$\Delta\theta_{\mathrm{BZO}}(^\circ)$
0BZO	11.65	0.15	1.89	0.36	16.1	
4BZO	11.71	0.22	1.98	0.46	16.6	1.14
2x4BZO	11.70	0.15	1.88	0.32	15.2	1.09
3x4BZO	11.70	0.15	1.89	0.33	15.0	1.08
4x4BZO	11.70	0.14	1.88	0.36	14.4	1.07
5x4BZO	11.70	0.16	1.87	0.35	14.3	1.14

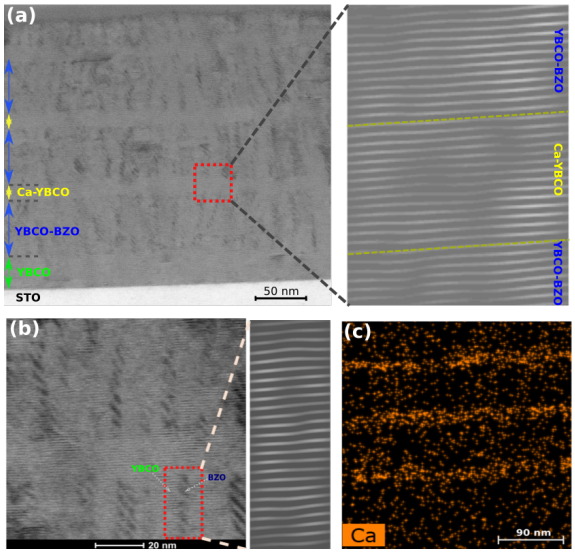

Fig. 2. (a) STEM image of the multilayer film with inverse FFT from the red square area shows the high-quality interface between Ca-doped YBCO and BZO-doped YBCO, highlighted by yellow dashed lines. (b) The magnified STEM image with inverse FFT from the red rectangular area displays the coherent interface between the YBCO matrix and BZO nanorod. (c) EDX mapping from (a) confirms that Ca is concentrated within the Ca-doped YBCO layers.

425 nm, respectively. Additionally, single-layer films of 0BZO and 4BZO, with thicknesses of approximately 280 nm and 285 nm, respectively, were deposited for comparative analysis.

The crystalline quality was assessed using x-ray diffractometry (XRD) performed on a PANalytical Empyrean diffractometer operating in Bragg-Brentano mode. Scanning transmission electron microscope (STEM) imaging were performed using a Thermo Fisher Scientific Osiris electron microscope (EMAT group, University of Antwerp) with bright-field (BF) detector operated at 200 kV at a camera length of 115 mm. The EDX-STEM datasets were acquired with a 233 pA beam current and a total time acquisition of ≈5 min. For the STEM measurements, a cross-sectional FIB lamella was prepared as described earlier [33].

The magnetic properties of the films were characterized using a Quantum Design Physical Properties Measurement System (PPMS). The critical temperatures were determined from ac magnetization curves, while the magnetic field dependencies of the critical current densities were obtained by employing the Bean model for rectangular films $J_c = 2\Delta m/[a(1 - a/3b)V]$, where Δm is the opening of the hysteresis loop, a and b are the width and the length of the film, and V is the volume of the film [34]. The accommodation field B^*, defined as the upper limit of the low-field plateau of $J_c(B)$, was determined using the criterion $J_c(B)/J_c(0) = 0.9$ [35]. Angular-dependent transport properties were measured over a 360° range at 40 K and a wide magnetic field range using the horizontal rotation option of the PPMS.

II. RESULTS AND DISCUSSION

A. Improved crystalline quality and microstructure

Analysis of the XRD results compiled in Fig. 1(b) and Table I reveals that the out-of-plane lattice parameter remains constant across all multilayers, closely mirroring the value observed in 4BZO. However, surprisingly the YBCO peak widths in all θ-, ϕ-, and ω-directions of the 4BZO multilayers are consistent with those of 0BZO and notably narrower than those of single layer 4BZO. This suggests that the Ca-YBCO layer aids in strain relaxation, restricts defect formation, and enhances the out-of-plane lattice ordering of YBCO, facilitating the growth of thicker BZO-doped YBCO layers with improved crystallographic properties through multilayering. Furthermore, examination of the $\Delta\theta$ values for the BZO(002) peaks indicates minimal variation in the BZO unit cells, suggesting optimal nanorod growth in the 4x4BZO sample. Additionally, the intensity ratio of the peak $I(005)/I(004)$ decreases in the multilayers, and with an increasing number of layers, signifying an improvement in the degree of oxidation within the YBCO lattice facilitated by multilayering.

As indicated by the STEM analysis in Fig. 2, BZO nanorods with a diameter of ≈5 nm and an average distance of ≈15 nm

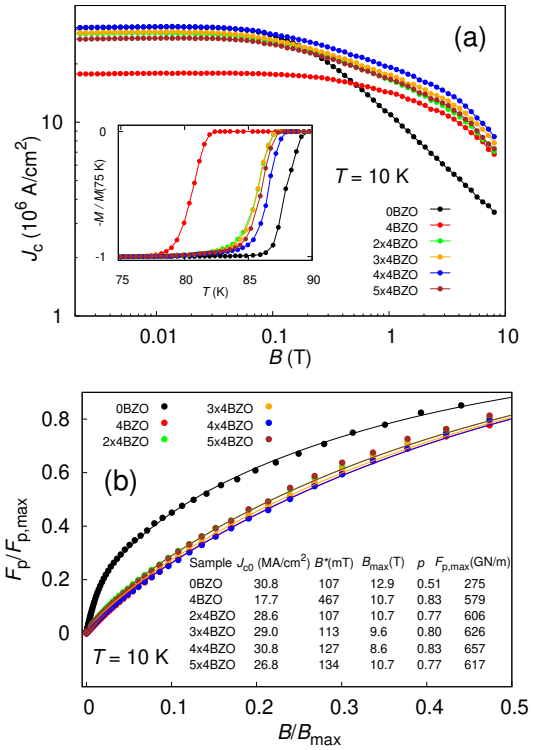

Fig. 3. (a) Magnetic field dependencies of J_c measured at 10 K up to 8 T, along with normalized ac magnetizations (inset), for both multilayer structures and single-layer films. (b) Magnetic field-dependent pinning force data $F_p(B)/F_{p,max}$, accompanied by $J_c(0)$ and accommodation field B^* values, as well as fitting parameters B_{max}, $F_{p,max}$, and p, which are associated with actual flux pinning.

extend through the BZO-doped YBCO layer, originating directly from the layer interface without the presence of a distorted region typically observed in single BZO-doped YBCO layers on various substrates [21]. Both the Ca-doped and BZO-doped YBCO layers are strained, but the overall lattice mismatch between these layers is relatively small. This is because Ca doping modifies the lattice parameters of YBCO, making them more compatible with BZO-doped YBCO. Although the interface quality between the BZO nanorods and the YBCO matrix varies significantly, it can be relatively coherent, as illustrated in Fig. 2(b). Furthermore, the EDX mapping analysis (Fig. 2(c)) indicates that elemental Ca is concentrated within the Ca-doped YBCO layers, with no evidence of Ca diffusion to the interface between the BZO nanorods and the YBCO matrix [37].

B. Effect of multilayering on superconducting properties

The temperature-dependent ac susceptibilities reveal that the multilayering of 4BZO with Ca-YBCO significantly elevates T_c, nearly reaching the level of 0BZO with $T_{c,onset} \approx 89.7$ K, as depicted in the inset of Fig. 3(a). Notably, the $T_{c,onset}$ obtained from resistivity measurements for 0BZO is 90.1 K, while for the 4BZO film and all multilayers, it is approximately 89 K.

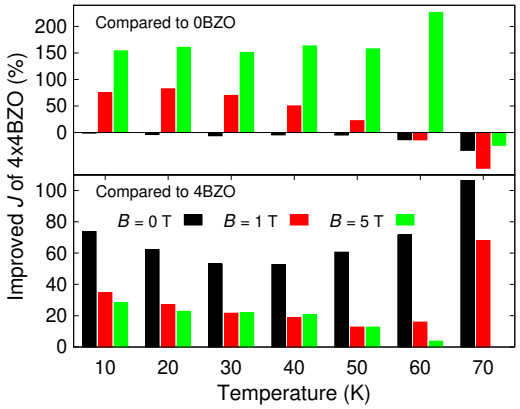

Fig. 4. Enhancement of J_c in the 4x4BZO multilayer structure at various temperatures and magnetic fields (0, 1, and 5 T), compared to single-layer samples 0BZO and 4BZO.

Upon examining the $J_c(B)$ curves at 10 K depicted in Fig. 3(a), notable differences emerge in the pinning performance profiles above the low-field plateau between 0BZO and 4BZO [38], [39]. Conversely, the $J_c(B)$ curves of the multilayer structures fall between these two samples. While the low-field $J_c(0)$ is akin to that of 0BZO, the shape of the high-field range resembles that of 4BZO. Although the $J_c(0)$ may surpass that of 0BZO, reaching its maximum in the 4x4BZO sample, the increase in B^* is marginal, as illustrated in Fig. 3(b). Furthermore, by fitting the scaled pinning force function with the Dew-Hughes formula [40] $F_p/F_{p,max}$ using $F_p(B) = BJ_c(B)$ [41], [42], we ascertain that both the maximum pinning force and the flux pinning exponent p attain peak values in the 4x4BZO sample. As shown in Fig. 4, the 4x4BZO sample exhibits clear superiority over 0BZO in high magnetic fields, exceeding 200% improvement, particularly at 60 K. Similarly, when compared to the 4BZO sample, the 4x4BZO sample outperforms it across the entire magnetic field range, with the most significant enhancement exceeding 100% observed in the zero-field region. These results clearly support the observed structural improvements in crystalline quality in the multilayered 4BZO films, resulting in a remarkable enhancement of $J_c(0)$.

As shown in Fig. 5, multilayering improves the high-field I_c across the entire angular range. At the relatively high temperature of 40 K, the highest absolute I_c is achieved in the 4xBZO sample, while in the 5xBZO sample, I_c decreases despite the increased overall thickness. However, the 4xBZO and 5xBZO samples exhibit the best I_c isotropy.

C. Suggested mechanisms for improved film growth

To understand the significance of growth mechanisms in enhancing superconducting properties, we must first examine the mechanisms that improve crystalline quality, which is directly linked to critical temperature and self-field $J_c(0)$ (Fig. 6). Previous experimental and theoretical studies have demonstrated that the crystalline quality of YBCO thin films can be enhanced through multilayering. This approach can extend the electron mean free path, thereby increasing $J_c(0)$

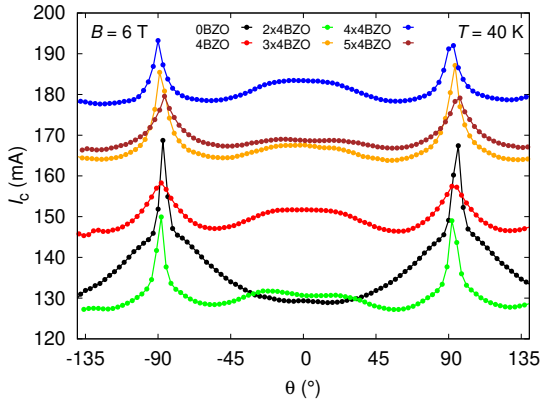

Fig. 5. Angular-dependent I_c measured at 40 K and 6 T. The angles $\theta = \pm 90^\circ$ correspond to the YBCO ab-plane, while $\theta = 0^\circ$ corresponds to the c-axis.

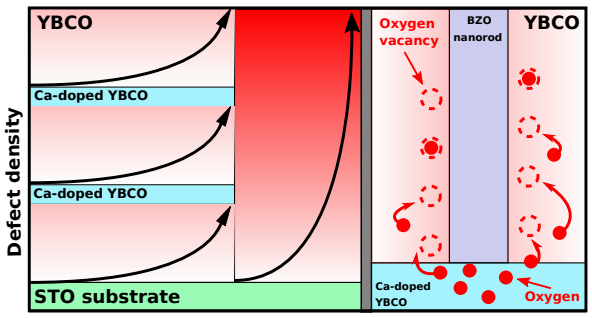

Fig. 6. Schematic illustration of the proposed mechanisms behind the improved crystalline quality and the resulting increase in $J_c(0)$. The left diagram depicts the effect of multilayering with Ca-doped YBCO intermediate layers, which influence strain relaxation and reduce absolute defect formation when compared with the single layer film. The right diagram shows how the diffusion of mobile oxygen atoms from the Ca-doped YBCO layer can compensate for strain-induced oxygen vacancies in the vicinity of BZO nanorods.

[13], [16], [18]. Multilayer structures allow for precise control over critical factors such as uniform and non-uniform strain relaxation. Techniques such as incorporating a CeO_2 interlayer or periodically interrupting film growth with sequential vacuum treatment are examples of this approach. Additionally, the underlying Ca-doped YBCO layer has been found to provide an optimal foundation for depositing the 4% BZO-doped YBCO layer. This is primarily due to its highly compatible lattice parameters, which create a smooth and epitaxial interface.

Ca-doped interlayers can also improve the weakened YBCO properties in the environment of BZO nanorods. Particularly, the partial substitution of Ca^{2+} ions for Y^{3+} in YBCO has been found to alter the carrier concentration, affecting the charge transfer from the CuO chains to the conducting CuO_2 planes [43], [44]. This substitution is counterbalanced by oxygen defects, slightly reducing the equilibrium oxygen content and lowering the superconducting transition temperature [45]. However, various aliovalent atomic substitutions in YBCO have been shown to increase the oxygen diffusion rate by up to a factor of 100 [43], [44]. Significant strain and misfit dislocations at the interface between BZO nanorods and the YBCO matrix lead to increased oxygen vacancy concentration [46], [47]. Thermodynamically driven mobile oxygen can migrate into these vacant sites, modifying the distorted BZO/YBCO interface closer to the optimal YBCO state. This concept aligns well with the XRD results, where the lower intensity ratio observed in the multilayer structures (Table I) indicates a higher oxygen concentration within the YBCO matrix.

D. Effect of crystalline quality on critical current density

The field dependence of critical current density at a fixed temperature can be generally described by the relation $J(B) \propto J_{c,0} \cdot B^{-\alpha}$, where $J_{c,0}$ is the zero-field (temperature limited) critical current and $\alpha \in \mathbb{R}^+$ is an unitless parameter associated with vortex pinning. The value of $J_c(B)$ is ultimately determined by the strongly correlated parameters $J_{c,0}$ and α. Consequently, achieving the optimal J_c under given B requires one to find a balance between these two parameters.

Improvement in vortex pinning (decreasing α) via inclusion of coherent artificial pinning centers (APC) within the YBCO matrix unavoidably comes with a cost of decreased $J_{c,0}$ and vice versa. This ultimately results from two distinct mechanisms; i) degradation of the crystalline quality of the superconducting lattice and ii) reduced superconducting cross-sectional area. While the crystalline quality can be maximized (in theory) via optimized choice of materials and deposition processes, the APC limited cross-sectional area for the supercurrent to pass through ultimately limits the $J_{c,0}$. However, one is technically able to increase this limit in carefully optimized YBCO/YBCO+APC bilayer films that are associated with an increased effective superconducting cross-sectional area when compared with standard YBCO+APC single layer films [14], [19], [20]. This, of course, comes at the cost of reduced vortex pinning efficiency, but our previous results indicate that one can afford to make this trade-off up to very high fields [21]. This effect can be considered to take place in the films studied herein, despite the used thickness of the APC-free film with respect to the overall film is significantly smaller when compared with the previously observed optimums. A more significant effect is likely be caused by the *seed-layer effect* [48], where the APC-free layer absorbs the substrate induced strain and consequently provides enhanced growth platform for the above deposited YBCO+BZO layers improving their crystalline quality.

The effect of crystalline quality to the $J_{c,0}$ can be understood via mean free path of the Cooper pairs (l) [10], [13]. In particular, degradation of the crystalline quality of YBCO reduces l by disrupting lattice periodicity and increasing electron scattering, which in turn affects the superconducting coherence length via the relation proposed by Pippard [49]

$$\frac{1}{\xi} = \frac{1}{\xi_0} + \frac{1}{l}, \tag{1}$$

where ξ_0 represents the clean limit superconducting coherence length. The l also modulates the coherence length by

$$\lambda = \lambda_0 \sqrt{1 + \frac{\xi_0}{l}}, \tag{2}$$

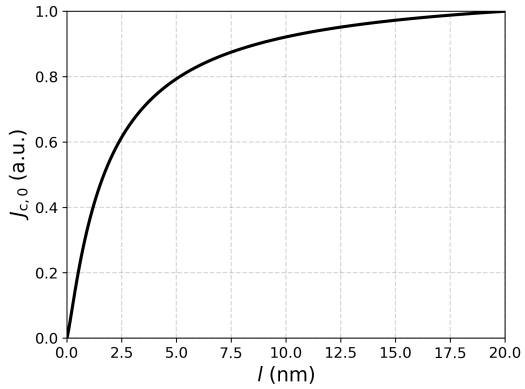

Fig. 7. The zero field critical current (normalized) as a function of the mean free path of the Cooper pairs calculated according to Eqs. (1)–(3). The calculated values of $J_{\mathrm{c},0}$ are normalized by dividing with the highest obtained $J_{\mathrm{c},0}$ within the interval $l \in [0\,\mathrm{nm}, 20\,\mathrm{nm}]$, where the upper limit is considered to be the limiting case of l in the studied samples based on the nanorod separations observed in the TEM images.

where λ_0 is again the clean limit value for the superconducting penetration depth. The values of the λ and the ξ ultimately determine the zero-field critical current density as [13]

$$J_{\mathrm{c},0} \propto \frac{1}{\lambda}\left[\frac{\Phi_0}{4\pi\mu_0\lambda^2}\cdot\left(\ln\left(\frac{\lambda}{\xi}\right)+\frac{1}{2}\right)\right]. \tag{3}$$

It should be pointed out that the depairing current (J_{dp}) is independent of l, and in practice the above defined $J_{\mathrm{c},0}$ limits the low-field performance of the YBCO films ($J_{\mathrm{c},0} \ll J_{\mathrm{dp}}$). Fig. 7 shows how the $J_{\mathrm{c},0}$ changes as a function of l. The plot is normalized by dividing the calculated datapoints with the highest obtained $J_{\mathrm{c},0}$ within the interval $l \in [0\,\mathrm{nm}, 20\,\mathrm{nm}]$, where the upper limit is considered to be the limiting case of l in the studied samples based on the ≈15 nm edge-to-edge separations of the BZO nanorods observed in the TEM images. The $J_{\mathrm{c},0}(l)$ increases steeply for $l < 5$, after its slope starts to saturate towards zero. However, the increase of l from 10 nm to 20 nm increases the $J_{\mathrm{c},0}$ approximately 10%. Comparing the scale of the nanorod separations observed in our samples with the $J_{\mathrm{c},0}(l)$ curve in Fig. 7, it is plausible that the coherence of the YBCO-BZO interface can have a significant effect on $J_{\mathrm{c},0}$ via l given the observed length scales. In our previous work [21], we have demonstrated how the Ca-doping (via layer structures) particularly improves the YBCO-BZO interface coherence consequently resulting in significant improvement of $J_{\mathrm{c},0}$. Moreover, we further concluded that this resulted in significant improvement in vortex pinning performance of the studied samples via increased the hopping potentials for the vortices between adjacent BZO-nanorods. This improved coherence between the YBCO-BZO interface thus suggests to be the main factor affecting the overall $J_{\mathrm{c}}(B)$ in the samples studied in this work.

Other mechanism behind the improved mean free paths of the Cooper pairs associated with our samples may include film relaxation effects between layer depositions. In our previous work [16], we concluded that our proposed *sequential vacuum-multilayering PLD deposition* technique resulted in significant improvement of the crystalline quality of intrinsic YBCO films when compared with conventional films deposited in a single setting. This was mainly attributed to the desorption of weakly bound atomic species, associated with crystalline imperfections in their vicinity, during the vacuum treatment. The resulting effect mimics the above mentioned *seed-layer effect* that results in improved growth conditions for following ablation interval. The vacuum-multilayering technique was observed to result in YBCO films with almost 40% improved $J_{\mathrm{c},0}$ when compared with films grown using the conventional PLD process. While multilayer films studied in this work were not vacuum treated between the ablation intervals, the same effect may still take place to some extent in any multilayer structures.

III. Conclusions

This study demonstrates that incorporating Ca-doped YBCO intermediate layers into BZO-doped YBCO multilayer structures significantly enhances the in-field critical current density and its isotropy. The improved crystalline quality and optimised distribution of BZO nanorods, particularly at lower temperatures and in mid-range magnetic fields, enable increased film thickness and greater current-carrying capacity. The proposed mechanisms are thoroughly discussed, highlighting how enhanced crystalline quality affects the electron mean free path of Cooper pairs and, consequently, the zero-field critical current density. These findings offer valuable insights for developing advanced YBCO coated conductors for various high-temperature superconducting power applications, suited to a range of temperature and magnetic field conditions.

References

[1] D. Larbalestier, A. Gurevich, D. M. Feldmann, and A. Polyanskii, "High-T_{c} superconducting materials for electric power applications," *Nature*, vol. 414, pp. 368–377, 2001.

[2] S. Kang, A. Goyal, J. Li, A. A. Gapud, P. M. Martin, L. Heatherly, J. R. Thompson, D. K. Christen, F. A. List, M. Paranthaman, and D. F. Lee, "High performance high-T_c superconducting wires," *Science*, vol. 311, pp. 1911–1914, 2006.

[3] C. V. Varanasi, J. Burke, L. Brunke, H. Wang, M. Sumption, and P. N. Barnes, "Enhancement and angular dependence of transport critical current density in pulsed laser deposited $YBa_2Cu_3O_{7-x}$+$BaSnO_3$ films in applied magnetic fields," *J. Appl. Phys.*, vol. 102, pp. 063 909:1–5, 2007.

[4] S. H. Wee, A. Goyal, Y. L. Zuev, and C. Cantoni, "High performance superconducting wire in high applied magnetic fields via nanoscale defect engineering," *Supercond. Sci. Technol.*, vol. 21, pp. 092 001:1–4, 2008.

[5] X. Obradors and T. Puig, "Coated conductors for power applications: materials challenges," *Supercond. Sci. Technol.*, vol. 27, pp. 044 003:1–17, 2014.

[6] A. C. Wulff, A. B. Abrahamsen, and A. Insinga, "Topical review: Multifilamentary coated conductors for ultra-high magnetic field applications," *Supercond. Sci. Technol.*, vol. 34, pp. 053 003:1–29, 2021.

[7] M. Z. Khan, E. Rivasto, H. Rijckaert, Y. Zhao, M. O. Liedke, M. Butterling, A. Wagner, I. Van Driessche, H. Huhtinen, and P. Paturi, "Strongly enhanced growth of high-temperature superconducting films on an advanced metallic template," *Cryst. Growth Des.*, vol. 22, pp. 2097–2104, 2022.

[8] G. Blatter, M. Feigel'man, V. Geshkenbein, A. Larkin, and V. Vinokur, "Vortices in high-temperature superconductors," *Rev. Mod. Phys.*, vol. 66, pp. 1125–1388, 1994.

[9] T. Matsushita, *Flux pinning in superconductors*. Springer, Heidelberg, Germany, 2007.

[10] E. F. Talantsev and J. L. Tallon, "Universal self-field critical current for thin-film superconductors," *Nat. Commun.*, vol. 6, pp. 7820:1–8, 2015.

[11] E. F. Talantsev, W. P. Crump, and J. L. Tallon, "Universal scaling of the self-field critical current in superconductors: from sub-nanometre to millimetre size," *Sci. Rep.*, vol. 7, pp. 10 010:1–15, 2017.

[12] A. Stangl, A. Palau, G. Deutscher, X. Obradors, and T. Puig, "Ultra-high critical current densities of superconducting $YBa_2Cu_3O_{7-\delta}$ thin films in the overdoped state," *Sci. Rep.*, vol. 11, pp. 8176:1–12, 2021.

[13] P. Paturi and H. Huhtinen, "Roles of electron mean free path and flux pinning in optimizing the critical current in YBCO superconductors," *Supercond. Sci. Technol.*, vol. 35, pp. 065 007:1–9, 2022.

[14] E. Rivasto, T. Hynninen, H. Huhtinen, and P. Paturi, "Optimization of high-temperature superconducting bilayer structures using a vortex dynamics simulation," *J. Phys. Cond. Mat.*, vol. 35, pp. 075 701:1–10, 2023.

[15] M. M. Aye, E. Rivasto, M. Z. Khan, H. Rijckaert, H. Palonen, H. Huhtinen, I. Van Driessche, and P. Paturi, "Multilayering BZO nanocolumns with different defect densities for YBCO high field applications," *New J. Phys.*, vol. 23, pp. 113 031:1–12, 2021.

[16] M. M. Aye, E. Rivasto, T. Vaimala, Y. Zhao, H. Huhtinen, and P. Paturi, "Improved crystalline quality and self-field J_c in sequentially vacuum-multilayered YBCO thin films on buffered metallic templates," *IEEE T. Appl. Supercond.*, vol. 33, pp. 6 601 806:1–6, 2023.

[17] A. V. Pan, S. V. Pysarenko, and S. X. Dou, "Drastic improvement of surface structure and current-carrying ability in yba$_2$ cu$_3$o$_7$ films by introducing multilayered structure," *Appl. Phys. Lett.*, vol. 88, p. 232506, 2006.

[18] A. Tuomola, E. Rivasto, M. M. Aye, Y. Zhao, H. Huhtinen, and P. Paturi, "Defining optimal thickness for maximal self-field J_c in YBCO/CeO_2 multilayers grown on buffered metal," *J. Phys. Cond. Mat.*, vol. 35, pp. 475 001:1–9, 2023.

[19] E. Rivasto, M. Todorovic, H. Huhtinen, and P. Paturi, "Optimization of high-temperature superconducting multilayer films using artificial intelligence," *New Journal of Physics*, vol. 25, pp. 113 046:1–15, 2023.

[20] E. Rivasto, M. M. Aye, H. Huhtinen, and P. Paturi, "Enhanced critical current density in optimized high-temperature superconducting bilayer thin films," *J. Phys. Cond. Mat.*, vol. 36, pp. 135 702:1–9, 2024.

[21] M. M. Aye, E. Rivasto, H. Huhtinen, and P. Paturi, "Enhanced critical current density in heterostructural YBCO/Ca-doped YBCO multilayers," *Cryst. Growth Des.*, vol. 24, pp. 4545–4555, 2024.

[22] X. Song, G. Daniels, D. M. Feldmann, A. Gurevich, and D. Larbalestier, "Electromagnetic, atomic structure and chemistry changes induced by Ca-doping of low-angle YBCO grain boundaries," *Nature Mat.*, vol. 4, pp. 470–475, 2005.

[23] G. Hammerl, A. Schmehl, R. R. Schulz, B. Goetz, H. Bielefeldt, C. W. Schneider, H. Hilgenkamp, and J. Mannhart, "Enhanced supercurrent density in polycrystalline $YBa_2Cu_3O_{7-\delta}$ at 77 k from calcium doping of grain boundaries," *Nature*, vol. 407, pp. 162–164, 2000.

[24] A. V. Pan, S. V. Pysarenko, D. Wexler, S. Rubanov, and S. X. Dou, "Multilayering and ag-doping for properties and performance enhancement in yba$_2$cu$_3$o$_7$ films," *IEEE T. Appl. Supercond.*, vol. 17, p. 3585, 2007.

[25] A. Goyal, S. Kang, K. J. Leonard, P. M. Martin, A. A. Gapud, M. Varela, M. Paranthaman, A. O. Ijadoula, E. D. Specht, J. R. Thompson, D. K. Christen, S. J. Pennycook, and F. A. List, "Irradiation free, columnar defects comprised of self-assembled nanodots and nanorods resulting in strongly enhanced flux pinning in $YBa_2Cu_3O_{7-\delta}$ films," *Supercond. Sci. Technol.*, vol. 18, pp. 1533–1538, 2005.

[26] J. L. MacManus-Driscoll, B. Maiorov, J. Durrell, S. Foltyn, Q. X. Jia, L. Civale, H. Wang, A. Kursumovic, and D. E. Peterson, "Guidelines for optimizing random and correlated pinning in rare-earth-based superconducting films," *Supercond. Sci. Technol.*, vol. 19, pp. S55–S59, 2006.

[27] S. R. Foltyn, L. Civale, J. L. MacManus-Driscoll, Q. X. Jia, B. Maiorov, H. Wang, and M. Maley, "Materials science challenges for high-temperature superconducting wire," *Nat. Mater.*, vol. 6, pp. 631–642, 2007.

[28] B. Maiorov, S. A. Baily, H. Zhou, O. Ugurlu, J. A. Kennison, P. C. Dowden, T. G. Holesinger, S. R. Foltyn, and L. Civale, "Synergetic combination of different types of defect to optimize pinning landscape using $BaZrO_3$-doped $YBa_2Cu_3O_7$," *Nat. Mater.*, vol. 8, pp. 398–404, 2009.

[29] M. M. Aye, M. Z. Khan, E. Rivasto, J. Tikkanen, H. Huhtinen, and P. Paturi, "Role of columnar defect size in angular dependent flux pinning properties of YBCO thin films," *IEEE T. Appl. Supercond.*, vol. 29, pp. 8 000 805:1–5, 2019.

[30] M. M. Aye, E. Rivasto, H. Rijckaert, H. Palonen, H. Huhtinen, I. Van Driessche, and P. Paturi, "Optimized $BaZrO_3$ nanorod density in $YBa_2Cu_3O_{6+x}$ matrix for high field applications," *Supercond. Sci. Technol.*, vol. 35, pp. 075 006:1–10, 2022.

[31] J. Wu and J. Shi, "Interactive modeling-synthesis-characterization approach towards controllable in situ self-assembly of artificial pinning centers in RE-123 films," *Supercond. Sci. Technol.*, vol. 30, pp. 103 002:1–15, 2017.

[32] M. Z. Khan, E. Rivasto, J. Tikkanen, H. Rijckaert, M. Malmivirta, M. O. Liedke, M. Butterling, A. Wagner, H. Huhtinen, I. Van Driessche, and P. Paturi, "Enhanced flux pinning isotropy by tuned nanosized defect network in superconducting $YBa_2Cu_3O_{6+x}$ films," *Sci. Rep.*, vol. 9, pp. 15 425:1–12, 2019.

[33] H. Rijckaert, "Preparation of the S/TEM lamella of commercial $REBa_2Cu_3O_{7-x}$ coated conductors by FIB," *IEEE T. Appl. Supercond.*, vol. 34, pp. 7 500 707:1–7, 2024.

[34] H. P. Wiesinger, F. M. Sauerzopf, and H. W. Weber, "On the calculation of J_c from magnetization measurements on superconductors," *Physica C*, vol. 203, pp. 121–128, 1992.

[35] C. Cai, B. Holzapfel, J. Hänisch, L. Fernandez, and L. Schultz, "Magnetotransport and flux pinning charactericties in RBaCuO (R=Gd,Eu,Nd) and $(Gd_{1/3}Eu_{1/3}Nd_{1/3})$BaCuO high-$T_c$ superconducting thin films on $SrTiO_3$," *Phys. Rev. B*, vol. 69, pp. 104 531:1–8, 2004.

[36] J. Ye and K. Nakamura, "Quantitative structure analyses of YBCO thin films: Determination of oxygen content from x-ray-diffraction patterns," *Phys. Rev. B*, vol. 48, pp. 7554–7564, 1993.

[37] V. Ogunjimi, M. A. Sebastian, D. Zhang, B. Gautam, J. Jian, J. Huang, Y. Zhang, T. Haugan, H. Wang, and J. Wu, "Enhancing magnetic pinning by bazro$_3$ nanorods forming coherent interface by strain-directed cadoping in yba$_2$cu$_3$o$_{7-x}$ nanocomposite films," *Supercond. Sci. Technol.*, vol. 34, p. 104002, 2021.

[38] A. Ichinose, K. Naoe, T. Horide, K. Matsumoto, R. Kita, M. Mukaida, Y. Yoshida, and S. Horii, "Microstructures and critical current densities of YBCO films containing structure-controlled $BaZrO_3$ nanorods," *Supercond. Sci. Technol.*, vol. 20, pp. 1144–1150, 2007.

[39] P. Mele, K. Matsumoto, A. Ichinose, M. Kukaida, Y. Yoshida, S. Horii, and R. Kita, "Systematic study of the $BaSnO_3$ insertion effect on the properties of $YBa_2Cu_3O_{7-x}$ films prepared by pulsed laser ablation," *Supercond. Sci. Technol.*, vol. 21, p. 125017, 2008.

[40] D. Dew-Hughes, "Flux pinning mechanisms in type ii superconductors," *Philosophical magazine*, vol. 30, p. 293, 1974.

[41] M. J. Qin, Z. X. Shi, H. L. Ji, X. Ji, X. X. Yao, H. C. Li, and X. S. Rong, "Paramagnetism and scaling behavior of volume flux pinning force density in a $GdBa_2Cu_30_{6+x}$ thin films," *J. Appl. Phys.*, vol. 78, pp. 3287–3292, 1995.

[42] C. V. Varanasi, P. N. Barnes, and J. Burke, "Enhanced flux pinning force and uniquely shaped flux pinning force plots observed in $YBa_2Cu_3O_{7-x}$ films with $BaSnO_3$ nanoparticles," *Supercond. Sci. Technol.*, vol. 20, pp. 1071–1075, 2007.

[43] J. L. Tallon, D. M. Pooke, M. P. Staines, M. E. Bowden, N. E. Flower, R. G. Buckley, M. R. Presland, and R. L. Davis, "Giant enhancement of oxygen mobility in high-T_c superconductors by atomic substitution," *Physica C*, vol. 171, pp. 61–68, 1990.

[44] J. T. Kucera and J. C. Bravman, "Transport characterization of calcium-doped YBCO thin films," *Phys. Rev. B*, vol. 51, pp. 8582–8590, 1995.

[45] Y. Zhao, H. K. Liu, and S. X. Dou, "Effect of co-doping of Ca and Al on hole concentration and superconductivity in the YBCO system," *Physica C*, vol. 179, pp. 207–213, 1991.

[46] C. Cantoni, Y. Gao, S. H. Wee, E. D. Specht, J. Gazquez, J. Meng, S. J. Pennycook, and A. Goyal, "Strain-driven oxygen deficiency in self-assembled, nanostructured, composite oxide films," *ACS Nano*, vol. 5, pp. 4783–4789, 2011.

[47] T. Horide, F. Kametani, S. Yoshioka, T. Kitamura, and K. Matsumoto, "Structural evolution induced by interfacial lattice mismatch in self-organized $YBa_2Cu_3O_{7-\Delta}$ nanocomposite film," *ACS Nano*, vol. 11, pp. 1780–1788, 2017.

[48] Y. Yao, W. Wang, L. Liu, S. Lu, X. Wu, T. Zheng, S. Liu, and Y. Li, "Effect of seed layer on the $Y_{0.5}Gd_{0.5}Ba_2Cu_3O_{7-\delta}$ film fabricated by pld," *Appl. Surf. Sci.*, vol. 442, pp. 658–663, 2018.

[49] A. B. Pippard, *Physica*, vol. 19, p. 765, 1953.